NASA Technical Memorandum 108794

A Comparison of Two Incompressible Navier-Stokes Algorithms for Unsteady Internal Flow

N. Lyn Wiltberger, Stuart E. Rogers, and Dochan Kwak
Ames Research Center, Moffett Field, California

November 1993

National Aeronautics and
Space Administration

Ames Research Center
Moffett Field, California 94035-1000

A COMPARISON OF TWO INCOMPRESSIBLE NAVIER-STOKES ALGORITHMS FOR UNSTEADY INTERNAL FLOW

N. Lyn Wiltberger, Stuart E. Rogers, and Dochan Kwak

Ames Research Center, Moffett Field, CA

SUMMARY

A comparative study of two different incompressible Navier-Stokes algorithms for solving an unsteady, incompressible, internal flow problem is performed. The first algorithm uses an artificial compressibility method coupled with upwind differencing and a line relaxation scheme. The second algorithm uses a fractional step method with a staggered grid, finite volume approach. Unsteady, viscous, incompressible, internal flow through a channel with a constriction is computed using the first algorithm. A grid resolution study and parameter studies on the artificial compressibility coefficient and the maximum allowable residual of the continuity equation are performed. The periodicity of the solution is examined and several periodic data sets are generated using the first algorithm. These computational results are compared with previously published results computed using the second algorithm and experimental data.

INTRODUCTION

In the field of computational fluid dynamics, it is challenging to obtain accurate results in a computationally efficient manner. A wide variety of approaches can be employed when solving a specific problem. This is particularly true of unsteady, incompressible methods; there are no time derivatives in the continuity equation, yet the velocity field must be divergence free at every time step. Manipulation of the governing equations must occur in order to formulate the problem. The current study compares two different incompressible Navier-Stokes algorithms to solve an unsteady, incompressible, internal flow problem. The first approach uses the artificial compressibility method introduced by Chorin (ref. 1) coupled with upwind differencing and a line relaxation scheme. The second approach uses a fractional step method (refs. 2 and 3) with a staggered grid, finite volume method. These two approaches have been widely used in recent work. As an example, in the 1991 10th AIAA Computational Fluid Dynamics Conference, a number of incompressible flow papers which used these methods were presented. A number of authors (refs. 4-9) used the artificial compressibility method in their work presented at this conference. An equal number of authors (refs. 8-13) used the fractional step method as a basis for their formulations.

Both methods have been used to compute the unsteady, viscous, incompressible, internal flow through a channel with a constriction. This specific problem was chosen for two reasons: one is the availability of experimental data for the problem; another is that this problem is geometrically simple but produces complex structures in the flow field for analysis. The physical applications of this problem include the area of bio-fluids research. Pulsatile flow through a channel with an obstruction models the phenomena of arteriosclerosis closely. This study provides not only the opportunity to perform code validation and comparison with experimental data, but generates results which may aid in a better understanding of the fluid dynamics associated with arteriosclerosis.

The current work includes a grid resolution study to determine an appropriate grid for the flow field analysis. A parameter study was performed on the artificial compressibility coefficient and its effect on solution convergence and accuracy. The solution was examined to determine the number of physical time steps needed to obtain a periodic solution. Solution accuracy and the effect of varying the maximum allowable tolerance for the divergence of velocity was investigated. Finally, the work was compared with the computational data of Rosenfeld (ref. 14) and the experimental results of Park (ref. 15).

The authors wish to thank Dr. Moshe Rosenfeld of MCAT Institute, San Jose, for his generous contributions of time and experimental results to this paper.

METHODS

The incompressible, unsteady, Navier-Stokes equations are known to be particularly difficult to solve. One of the reasons for this difficulty is the absence of a time derivative of pressure in the governing equations. Since the speed of sound in a truly incompressible fluid is infinite, the entire pressure field is affected instantaneously by a disturbance at any one point in the flow domain. This requires that the numerical algorithm propagate information through the entire flow domain during one discrete time step. Global coupling of the discretized system is implied, thus some type of iterative scheme is usually required to solve the equations in time. The elliptical nature of these equations causes the generation of time-accurate solutions to be computationally expensive.

Two different computational methods were employed to model the fluid dynamics of unsteady, incompressible, pulsatile channel flow: (1) an artificial compressibility method, and (2) a fractional step method. The fractional step data used for comparison in this study was generated separately by Rosenfeld (ref. 14), by the fractional step code, INS3D-FS (ref. 16). The INS3D-FS code utilizes an integral formulation of the Navier-Stokes equations and finite volume discretization to solve both steady-state and time-dependent flows. In this algorithm, the momentum equation is marched forward using the last known pressures to solve for the velocity field. The new velocity field at this point does not necessarily satisfy the continuity equation. A Poisson equation in pressure is then solved

to obtain the corrections to the velocity field such that the continuity equation will be satisfied; thus, the solution is advanced one time step. In practice, the Poisson equation is iterated until the maximum residual is less than 10^{-8}, where the residual is the divergence of velocity multiplied by the volume of the computational cell. A staggered mesh approach is used with the INS3D-FS code, which removes the need for artificial dissipation.

The code used by the authors to generate solutions was the INS2D code developed by Rogers (refs. 17 and 18). This code solves the incompressible Navier-Stokes equations in two dimensional generalized coordinates for both steady-state and time varying flows. The equations are formulated into a mixed set of hyperbolic and parabolic partial differential equations using the method of artificial compressibility. In this method, a pseudo-time derivative of pressure is added to the continuity equation:

$$\partial p/\partial \tau = -\beta \nabla \vec{U}$$

where p = pressure, τ = pseudo-time, $\vec{U}$ = velocity, and β is the artificial compressibility constant which controls the propagation of the artificial pressure waves. The convective terms are differenced using an upwind biased flux-difference splitting method. The discretized equations are solved using a line-relaxation scheme. This method uses sub-iterations in pseudo-time on the global system of equations as the mechanism to drive the divergence of velocity toward zero. In practice, the sub-iterations are terminated once the maximum divergence of velocity in the continuity equation is reduced below a specified constant, ε_{cont}. This constant can be much larger than machine zero; for instance, accurate solutions have been obtained (refs. 17 and 18) using values of $\varepsilon_{cont} = 10^{-3}$.

PROBLEM DEFINITION

The physical problem examined in this study was pulsatile flow through a channel with a constriction. The computational geometry is consistent with the experimental set-up of Park (ref. 15), and is shown in figure 1. The channel height is h and has been normalized to unity. The height of the constriction is given by $a = 0.57$. This is the distance from the top wall of the channel to the lowest point in the constriction. The length of the channel upstream of the constriction is given by $L_u = 7$. The length of the channel in which the constriction occurs is given by $L_c = 4.66$, and the downstream portion of the channel is given by $L_d = 15.34$. The total length of the channel is given by L_{total} and is equal to $L_u + L_c + L_d = 27.0$.

The computational boundary conditions were implemented as follows. For the upper and lower walls of the channel, no slip conditions were specified. The inflow boundary to the experimental set-up occurred at 100 channel heights upstream of the constriction. Since it would be computationally expensive to compute the flow for this entire domain, the computational inflow boundary was placed at seven channel heights upstream of the

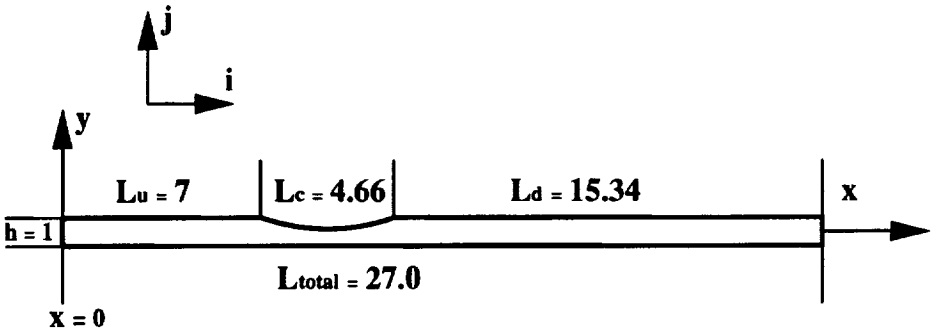

Figure 1. Physical description of computational geometry.

constriction. Previous work was done by Rosenfeld (ref. 14) to determine the appropriate inflow boundary conditions to match the experimental setup, and this information was used in the current work. A parabolic profile was imposed at the inflow boundary and the average inflow velocity was set to match the mass flow from the experimental setup. The average inflow velocity is periodic and given by the shape function in figure 2.

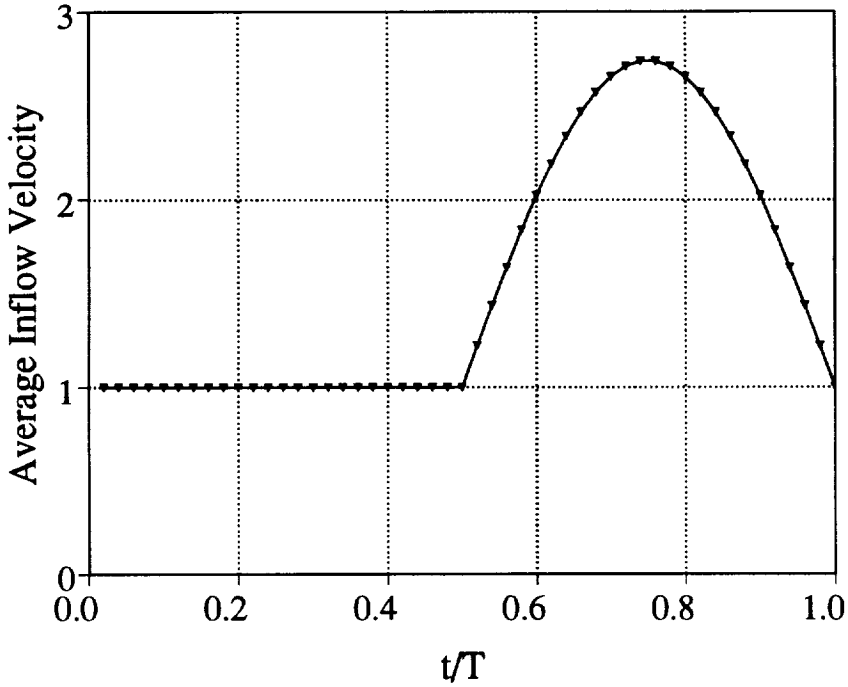

Figure 2. Average inflow velocity magnitude versus time for one period.

This shape is defined analytically by

$$U(t) = U_s \qquad 0 < t/T < 1/2$$
$$U(t) = U_s - U_p \sin(2\pi t/T) \qquad 1/2 < t/T < 1$$

where U_s is the non-dimensionalized steady component of the average inflow velocity, U_p is the pulsatile component and T represents the period. This waveform was chosen for the inflow velocity because it approximates the pulses in velocity that blood encounters during diastole and systole in mammalian circulatory systems and provides realistic conditions for the modeling of arteriosclerosis.

Associated with this problem, there are several relevant relationships between the physical parameters which govern this flow.

$$Re_s = \frac{U_s h}{\nu}$$
$$f_p = \frac{Re_s}{T}$$
$$St = \frac{h}{U_p T}$$
$$U_p = \frac{h f_p}{St Re_s}$$

Re_s is the Reynolds number for the flow, U_s is the steady component of the average inflow velocity, h is the non-dimensionalized height of the channel, and ν is the kinematic viscosity of the fluid. The frequency of the period T is given by f_p. The Strouhal number is given by St, where h is the channel height, and U_p is the pulsatile component of the average inflow velocity. These physical parameters were specified to correspond with the computational work done by Rosenfeld (ref. 14), and the experimental work done by Park (ref. 15).

The outflow boundary conditions specified in the work by Rosenfeld (ref. 14) were of the non-reflecting type with the streamwise derivative of velocity set to zero, $\partial u/\partial x = 0$. In the present work, a non-reflecting boundary condition was used based on the method of characteristics to solve for the velocity; the static pressure was specified to be constant.

To compare the computed results from the two algorithms on an equal basis, the grids used to model this geometry matched the grids used by Rosenfeld (ref. 14). A coarse mesh was generated with 97×21 grid points and clustering near the upper and lower walls and in the regions where large gradients were expected, resulting in 70 percent of the grid points being clustered in the vortical region downstream of the constriction. From this mesh, medium, fine, and ultra-fine grids were generated by doubling the points in each of the i and j directions, as defined in figure 1, for each level of refinement. This resulted in four grids with an increasing number of grid points: a coarse grid with 97×21 grid points, a medium grid with 193×41 grid points, a fine grid with 289×61 grid points, and an ultra-fine grid with 385×81 grid points. Figure 3 shows part of the coarse mesh near the constriction.

A baseline case was first calculated from which further parametric studies were performed. This case shall be referred to as Case I, and the constants specified are: the Reynolds number $Re_s = 131.9$, the depth of the constriction $a/h = 0.57$, the Strouhal number $St = 0.42$, the pulsatile component of the average inflow velocity $U_p = 1.217$, and the period $T = 1.957$ seconds in physical time.

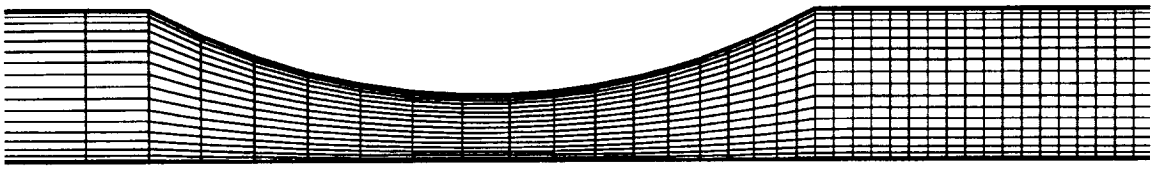

Figure 3. 97 × 21 coarse mesh in the area of the constriction.

COMPUTED RESULTS

First, a grid resolution study was performed using all four grids and the parameters of Case I. To obtain a starting solution for each of the grids, a converged steady-state solution was obtained. The calculation was restarted with time-varying pulsatile inflow from the steady-state solution and run out for four periods with a value of $\beta = 50,000$ and $\Delta t = 0.03914$. Grid convergence was analyzed using two physical parameters: the distribution of skin friction on the bottom wall of the channel, and the static pressure at the centerline of the channel. As these are laminar calculations, the skin friction coefficient, C_f, is normalized by the Reynolds number and is given by

$$C_f = \frac{\tau_w}{1/2\rho U_s^2}$$

where τ_w is the shear stress at the wall and ρ is the density. The skin friction coefficient and pressure at the centerline of the channel are shown at the beginning of the period, t/T = 0.0, for all four cases shown in figures 4(a)-(b) and 5(a)-(b). From the figure, it is apparent that the solutions are close to being grid independent for the two finest meshes, as the solution from the 289 × 61 mesh is close to the solution from the 385 × 81 mesh. However, 30 percent less CPU time is needed to generate a solution for a 289 × 61 mesh than for the 385 × 81 mesh. This geometry produces a solution with many strong flow gradients. Flow is produced which is continuously reversing throughout the channel which creates strong streamwise pressure gradients and strong vorticity gradients near the walls. A grid with relatively fine spacing is needed to adequately capture all of the important flow physics which are inherent in this problem. As a result, the 289 × 61 grid was chosen to use in the remainder of the calculations in the study. Rosenfeld (ref. 14) performed a grid resolution study and determined that a nearly grid independent solution was also obtained with the fractional step method for the 289 × 61 grid.

An in-depth examination of the skin-friction and pressure data, shown in figures 4(b) and 5(b), reveals several "spikes" in the INS2D solution near the beginning and end of

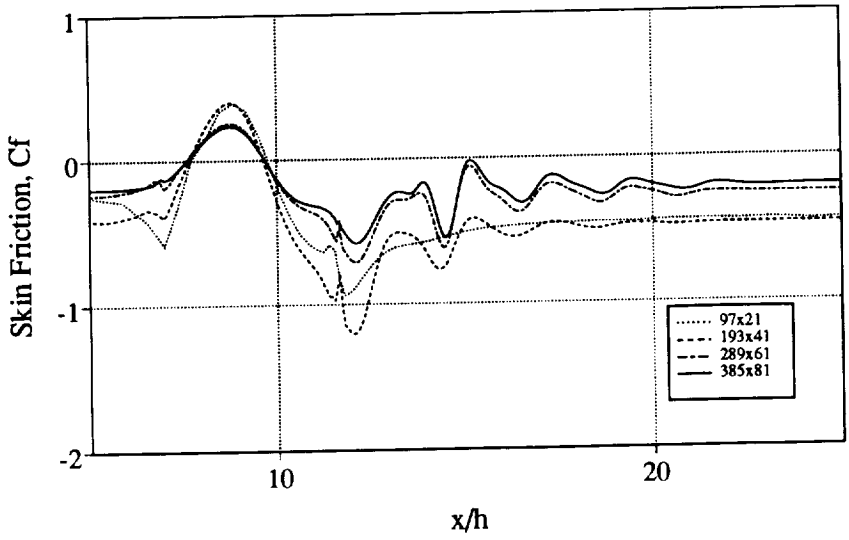

Figure 4(a). Effect of grid resolution on skin friction at the lower wall.

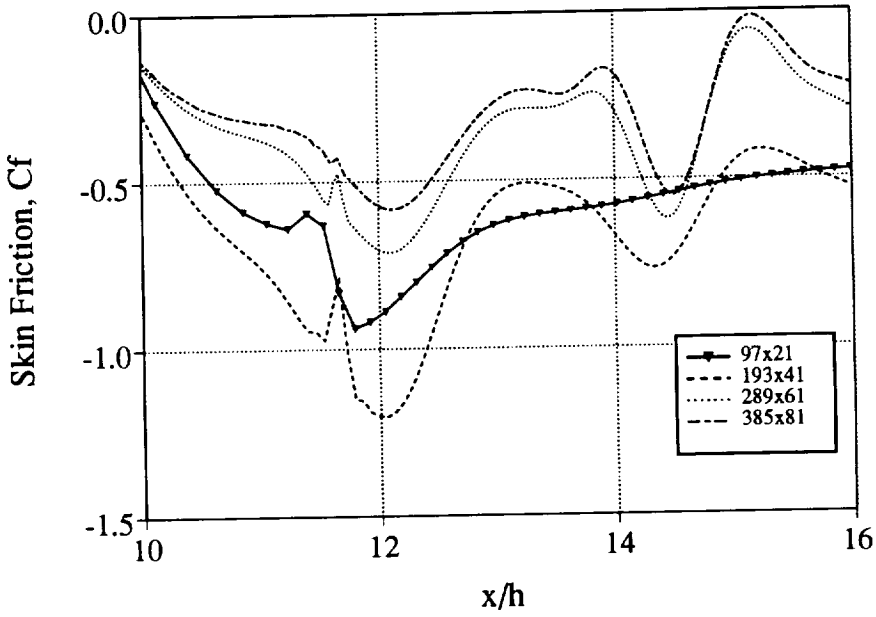

Figure 4(b). Close-up of figure 4(a), in the area of the constriction.

the constriction. In these figures, the magnitude of spikes appears to diminish as the grids become more refined. The magnitude of the spikes in the solutions was also affected by the choice of β, the artificial compressibility coefficient, used in running the INS2D code. This dependence on β is discussed in the following section.

A parametric study on the effects of different values of β on the speed of solution convergence was performed. The values of β used ranged from 50,000 to 0.1 by an order of magnitude for each case. When running the INS2D code, the use of different values of β

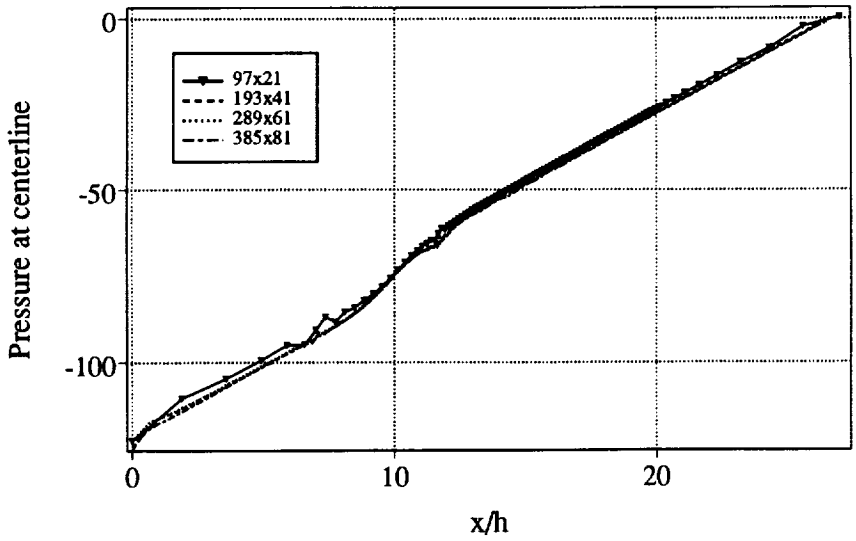

Figure 5(a). Effect of grid resolution on centerline pressure.

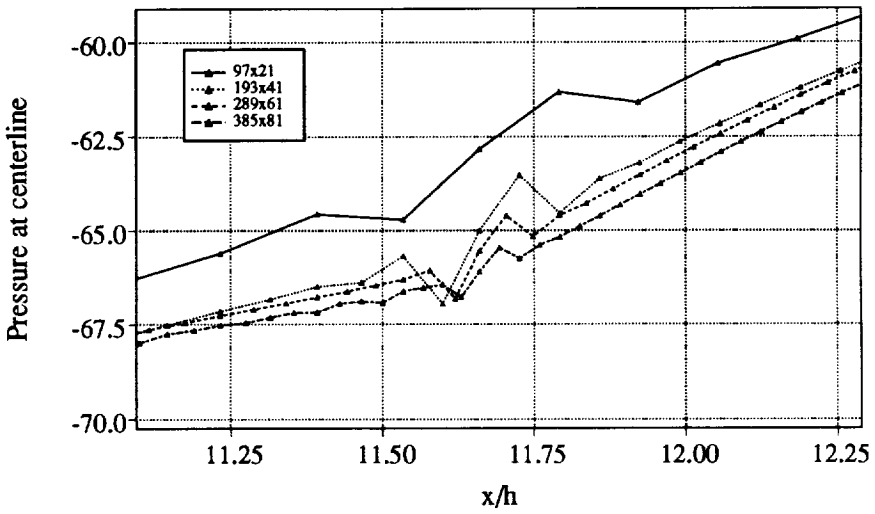

Figure 5(b). Close-up of figure 5(a), in area of constriction.

will generate basically the same solution with minor differences, but will greatly affect the speed of convergence and therefore the amount of CPU time needed to obtain a solution. This occurs because the number of sub-iterations that are calculated in pseudo-time in the unsteady mode are either increased or decreased depending on how a specific value of β propagates information within a specific geometric configuration. Figure 6 shows the effect of different values of β on CPU time; the data from these solutions is shown in figures 7(a)-(b) and 8(a)-(b). The use of a large β greatly enhances the speed at which the unsteady solution converges for this geometry, as shown in figure 6. However, in figures 7(a)-(b) and 8(a)-(b), which show the skin-friction coefficient at the lower wall and

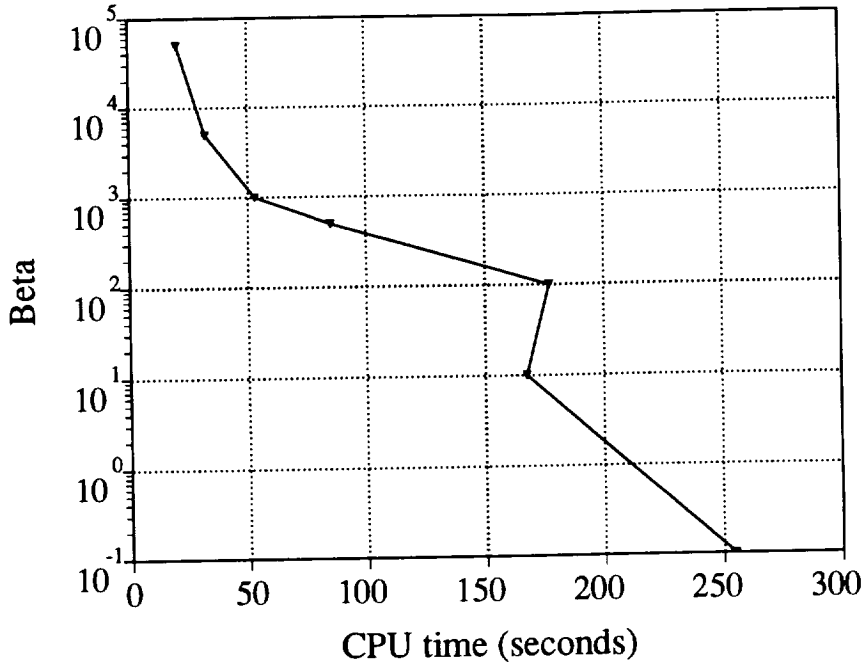

Figure 6. Effect of β on computing time needed for first half of period.

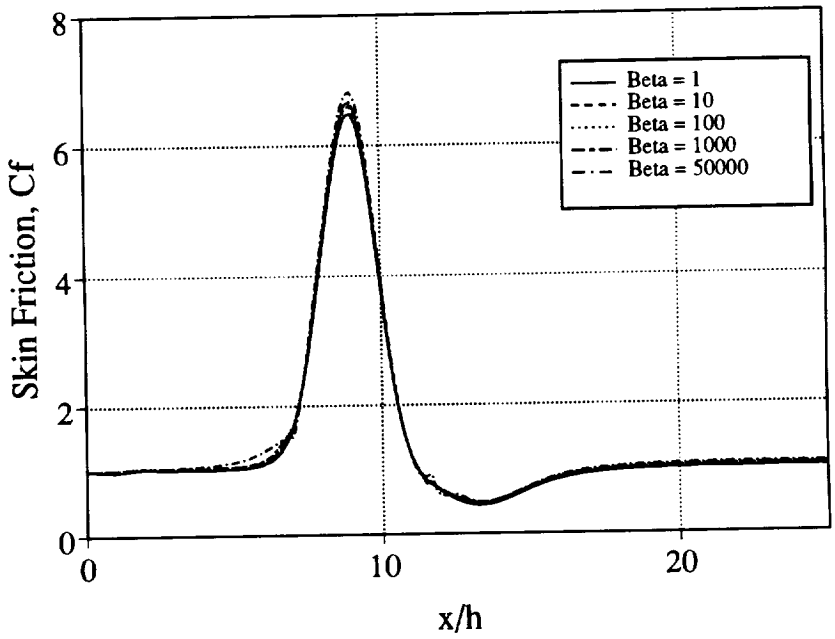

Figure 7(a). Effect of β on skin friction at the lower wall at $t/T = 0.5$.

pressure at the centerline of the channel at $t/T = 0.5$, the relative smoothness of the solution is adversely affected by the use of the large β. The pressure appears to be more adversely affected by the use of a large β than the skin-friction. Since the pressure term

in the continuity equation is scaled by β, small spikes in the velocity field produce large spikes in the pressure field. A value of $\beta = 10^3$ was chosen for use in the remainder of the study. This value produced reasonably fast convergence to a periodic solution and minimized the magnitude of the spikes in the solution.

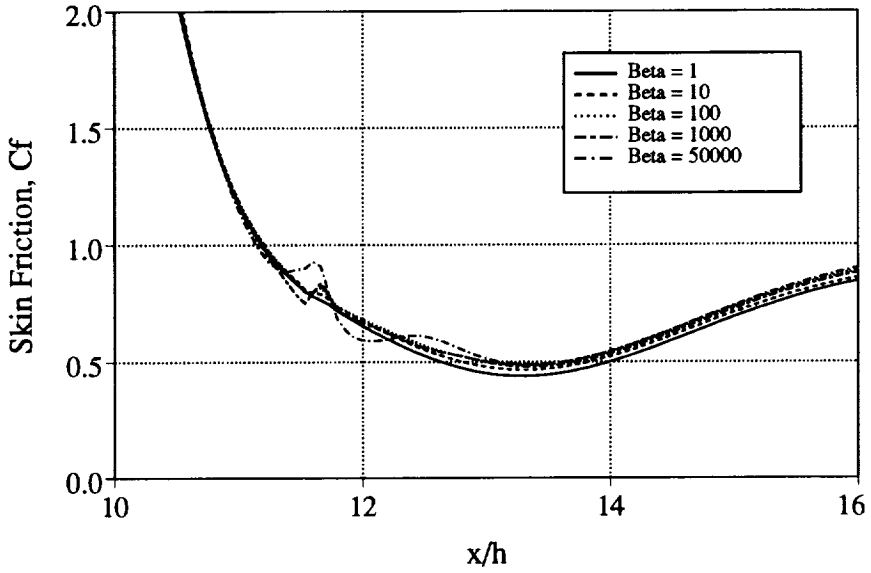

Figure 7(b). Close-up of figure 7(a), in the area of the constriction.

Several alternatives can be utilized to reduce the magnitude of the spikes in the solutions of the large β cases. Since the grid resolution study, shown in figures 4(b) and 5(b), shows that the use of a finer grid reduces the magnitude of the spikes, refining the grid in the area of the constriction could produce a smoother solution with the use of a larger β. This could be done without increasing the number of points in the grid by clustering the existing points in the constriction region. Also, smoothing of the grid was performed by fitting a cubic spline to the grid lines lengthwise at the beginning and end of the constriction. This smoothing did reduce the magnitude of the spikes for a case of $\beta = 50,000$, as shown in figures 9(a)-(b). However, since this is a validation study with the results of Rosenfeld (ref. 14), the remainder of this study was performed with the exact grids used in the work done by Rosenfeld (ref. 14) and not the smoothed grids.

The use a TVD limiting scheme is another method which may be employed to reduce the magnitude of the spikes when running the INS2D code with a large β. Using a TVD limiting scheme with the upwind differencing may add enough dissipation to smooth out these spikes, yet may also reduce the accuracy of the solution. Thus, the preferred correction for this case would involve refining the affected region of the grid.

The issues of periodicity and convergence of the solution were also examined in this study. When running a time dependent case with the INS2D code, a convergence critera

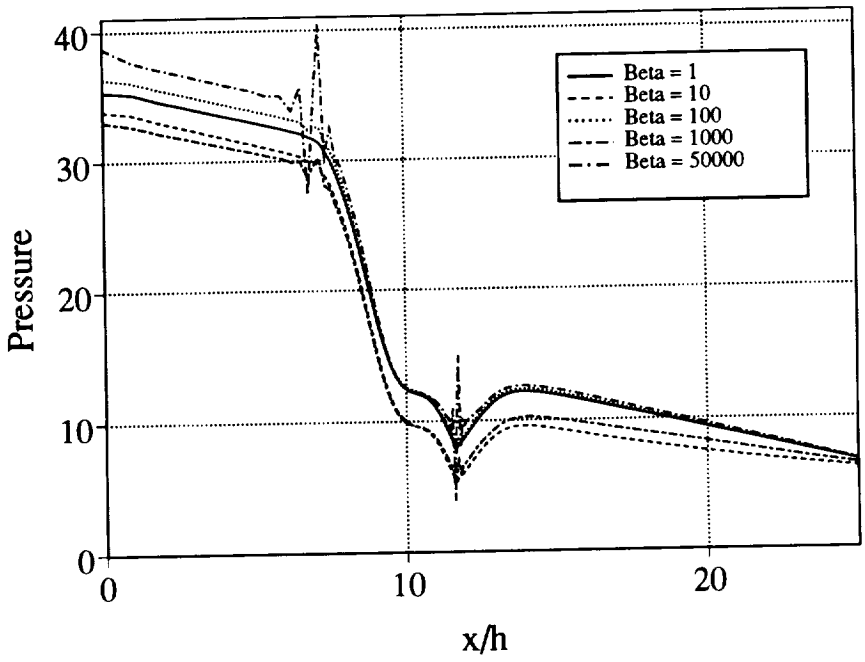

Figure 8(a). Effect of β on centerline pressure at $t/T = 0.5$.

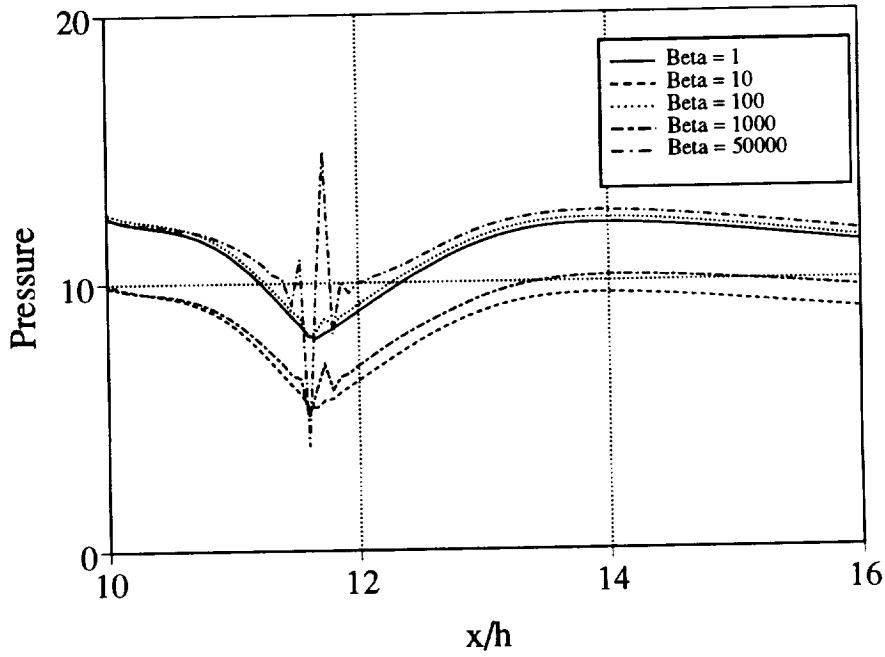

Figure 8(b). Close-up of figure 8(a), in the area of the constriction.

must be specified for the sub-iterations. The parameter ϵ_{cont}, the residual of the continuity equation, is used as the tolerance for the maximum divergence of velocity in the entire

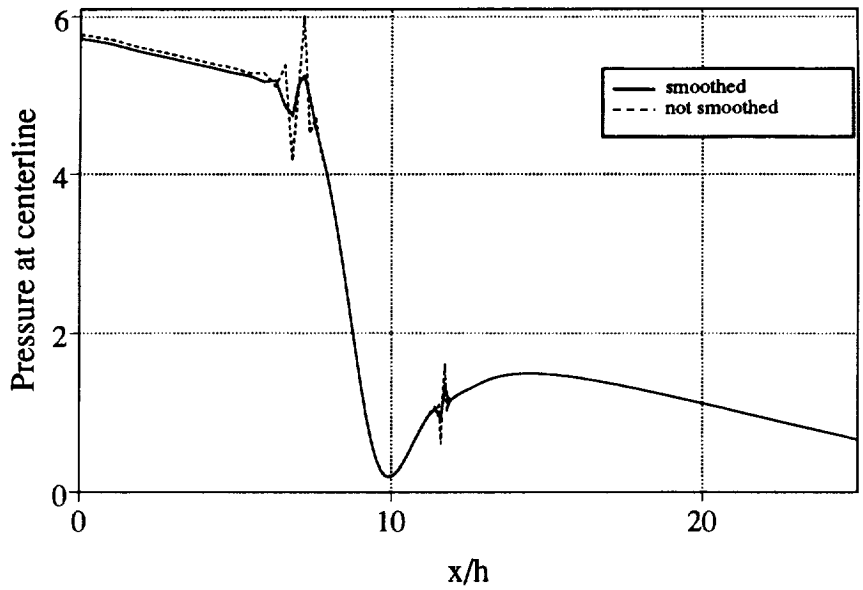

Figure 9(a). Smoothed versus non-smoothed grid for $\beta = 50,000$.

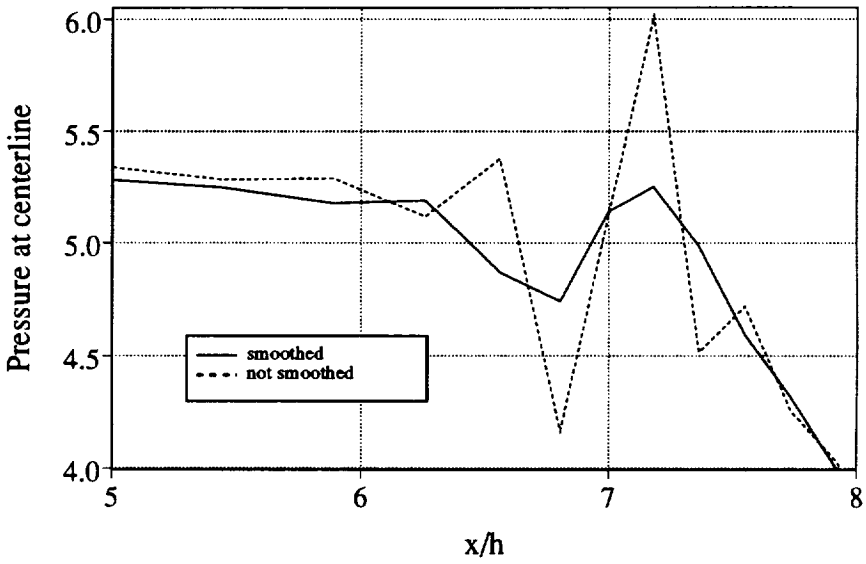

Figure 9(b). Close-up of figure 9(a), in the area of the constriction.

flow field; once the tolerance is reached, the sub-iterations are terminated and the code continues on to the next time level. The maximum divergence of velocity at each grid point was determined using a third order differencing scheme. A parameter study was performed to determine the appropriate value for ε_{cont} which would generate an accurate periodic solution for the least amount of computer time. The value of ε_{cont} was varied by an order of magnitude for four cases from 10^{-1} to 10^{-4}. Solutions were generated for each value of ε_{cont} for 10 consecutive periods. The solutions were checked for periodicity by taking the

root mean square (RMS) of the difference over each grid point of the dependent variables between subsequent periods. A direct correlation exists between the decrease in these RMS values and the solution periodicity. Figure 10 shows the effect of ε_{cont} on the periodicity of the solutions. As shown in figure 10, running the INS2D code with a value of ε_{cont} of 10^{-3} produces the solution with the smallest RMS value consistently throughout the ten periods. Figure 11 shows the same data plotted against CPU time instead of periods. Each order of magnitude decrease in ε_{cont} produced a factor-of-two increase in the number of sub-iterations within one time step, and therefore increased the amount of CPU time needed to obtain a solution. Values of ε_{cont} of 10^{-3} and 10^{-4} generated the more periodic solutions, but a value of $\varepsilon_{cont} = 10^{-3}$ produces a smaller RMS error than $\varepsilon_{cont} = 10^{-4}$; this translates to faster convergence to periodicity, while using approximately 40 percent less CPU time. The value of ε_{cont} of 10^{-3} was used in the remainder of the study.

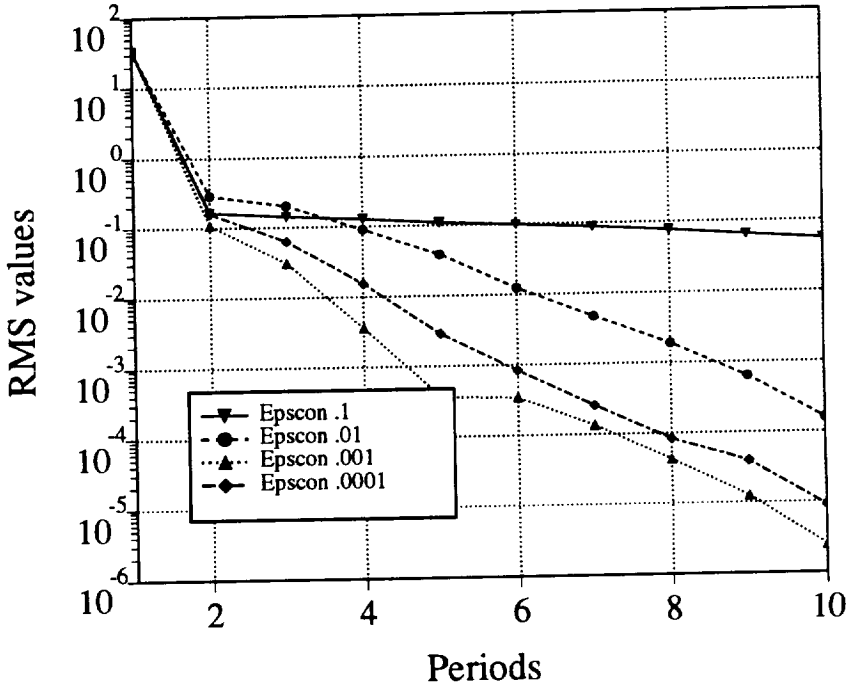

Figure 10. Effect of ε_{cont} on periodicity: root mean square of change in dependent variables versus period.

Once the basic operational parameters had been established for running the INS2D code with this configuration, two cases were run to generate data which were used to compare with Rosenfeld's (ref. 14) computational data and Park's (ref. 15) experimental data. The geometry remained the same for the two cases, but the inflow conditions vary and are given in table 1.

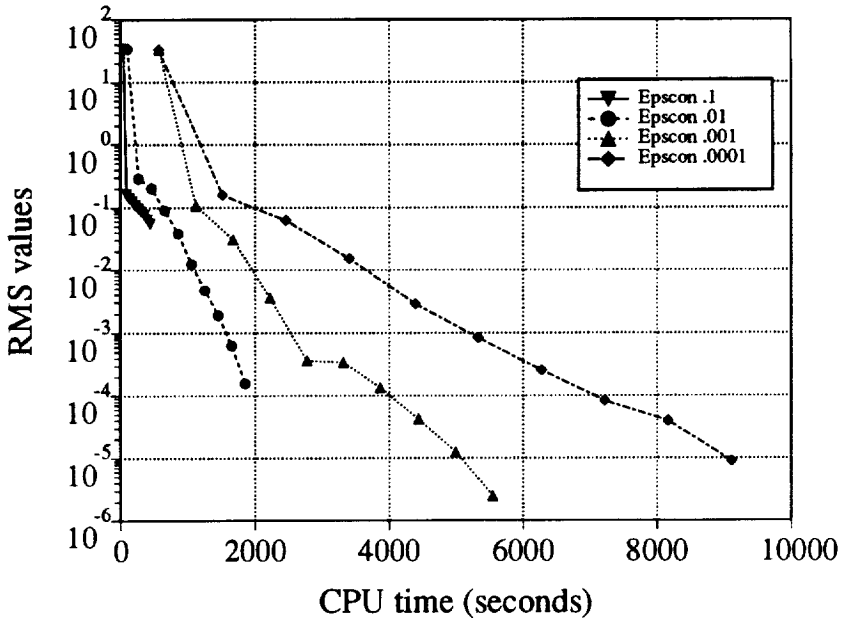

Figure 11. Effect of ε_{cont} on periodicity: root mean square of change in dependent variables versus CPU time.

Table 1. Parameters used for comparison study

Parameter	Case I	Case II
Re_s	131.9	138.3
a/h	0.57	0.57
T	1.957	1.368
St	0.42	0.42
U_s	1.5	1.5
U_p	1.217	1.740

A converged periodic solution was generated for both of these cases. Data was saved at each time step in the period for comparison with Rosenfeld (ref. 14) and Park (ref. 15). Figures 12(a)-(d) show the coefficient of skin friction on the lower wall for both the current results using the INS2D code and Rosenfeld's (ref. 14) work using the INS3D-FS code, at various times during the period for Case I. A comparison of the computational data shows that the solutions appear to match with respect to location of skin friction maxima and minima. However, the data generated using the INS3D-FS code has a larger fluctuation in skin friction values in the region just behind the constriction than the data generated using the INS2D code. This correlates to stronger vorticity in these regions in the solution generated by the INS3D-FS code.

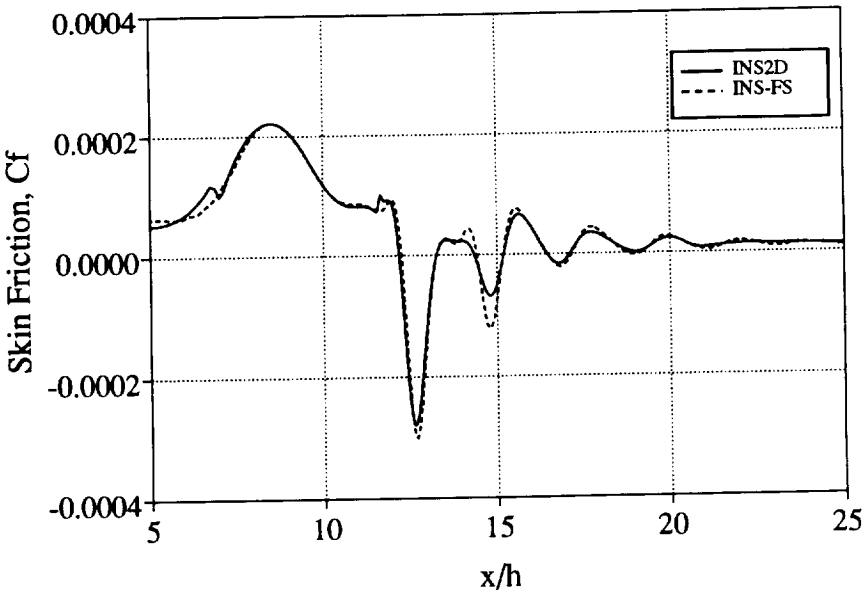

Figure 12(a). Comparison of INS2D and INS3D-FS results: computed skin friction at the lower wall at $t/T = 0.24$.

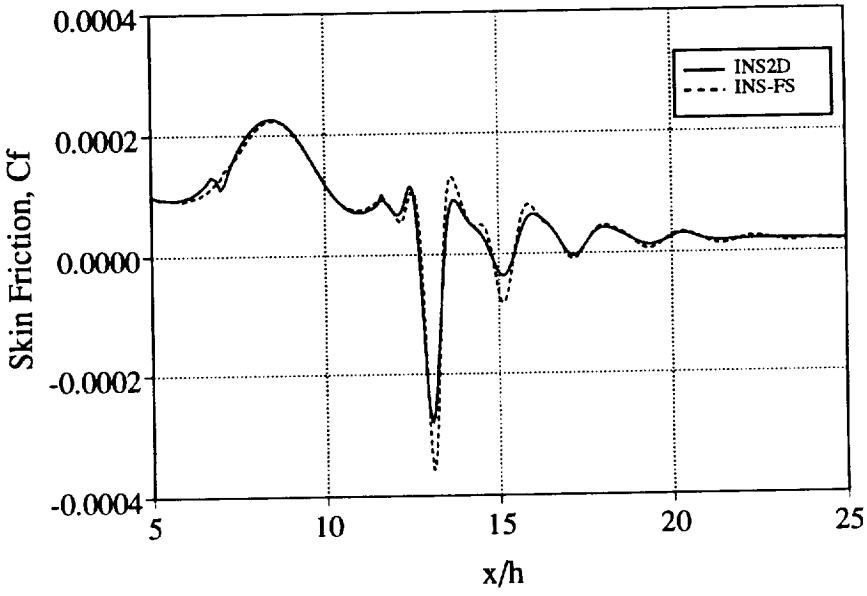

Figure 12(b). Comparison of INS2D and INS3D-FS results: computed skin friction at the lower wall at $t/T = 0.5$.

The INS2D code was also used to compute instantaneous streamlines for Case I. These streamlines are compared with streamlines generated using the INS3D-FS code for

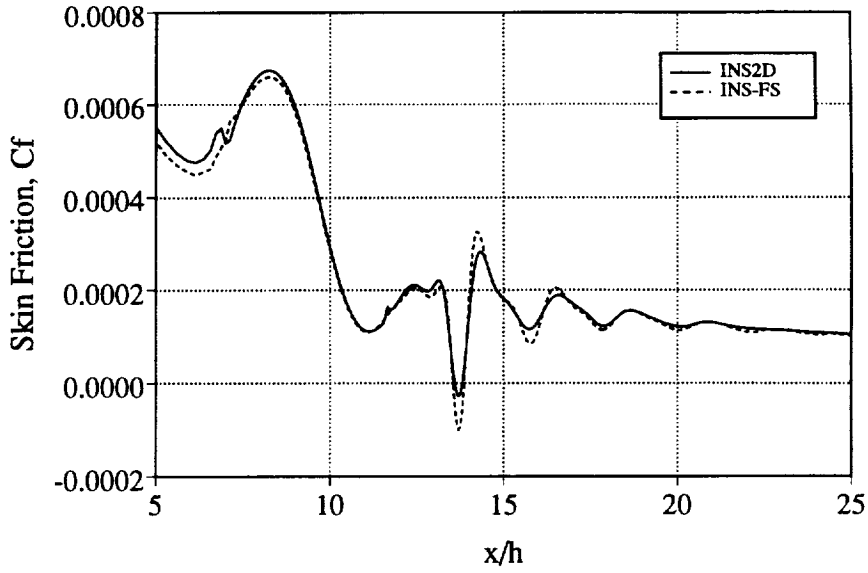

Figure 12(c). Comparison of INS2D and INS3D-FS results: computed skin friction at the lower wall at $t/T = 0.74$.

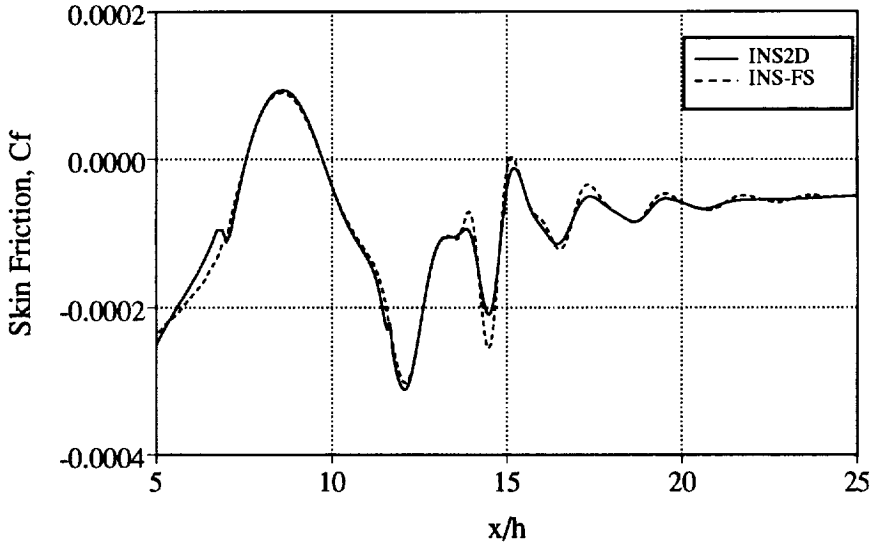

Figure 12(d). Comparison of INS2D and INS3D-FS results: computed skin friction at the lower wall at $t/T = 1.0$.

Case I and are shown at $0.1T$ intervals throughout the period in figures 13 and 14. The streamline plots illustrate the same phenomena as the skin friction plots, that the results generated by the INS3D-FS code have larger vortical structures behind the constriction

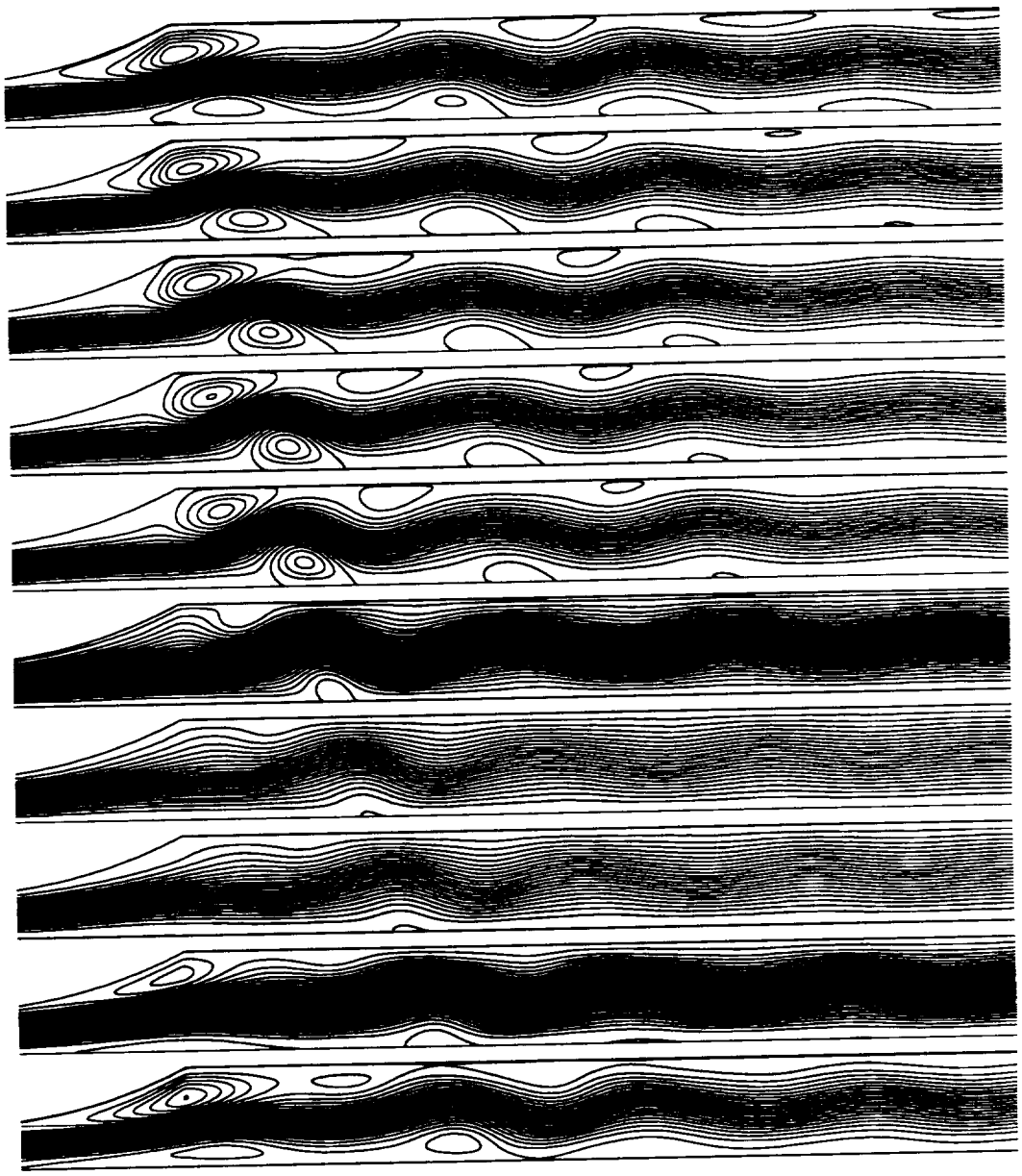

Figure 13. INS2D results: streamline data at $0.1T$ intervals from $0.1T$ to $1.0T$.

throughout the entire period, even during the pulse in the inflow average velocity, as shown in frame 7 at $0.7T$ in figures 13 and 14, when most of the vortical structures are washed out.

Another easily quantified physical result was the location of the center of the B-vortex. The B-vortex is defined to be the vortex along the bottom wall of the channel; it grows immediately behind the end of the constriction and is shed downstream. The location of this vortex was examined as function of time and the results were compared with the INS3D-FS code results and the experimental results for both Case I and Case II. The

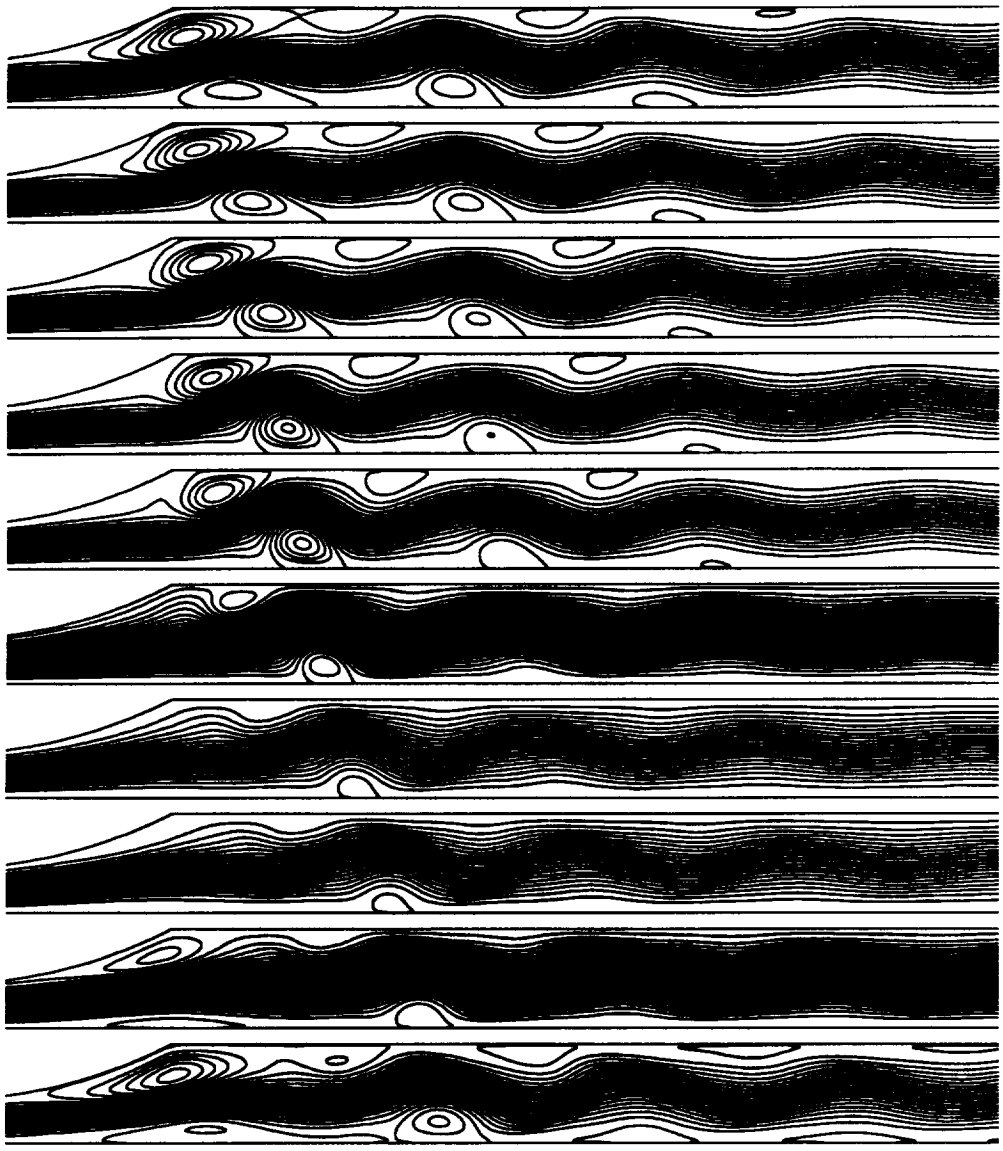

Figure 14. INS3D-FS results: streamline data at $0.1T$ intervals from $0.1T$ to $1.0T$.

location of the center of the B-vortex can be found by plotting the instantaneous streamlines with a fine increment of the contour lines. This is analogous to the measurement of the experimental vortex location, which was measured using flow visualization pictures. Figures 15 and 16 show the results given by Rosenfeld (ref. 14), the computed results from this study, and the experimental results. There is good agreement between the computed results by the INS3D-FS code and the INS2D code. The agreement with experimental data is fairly good for $t/T < 2.0$ for the two cases, but declines in quality for $t/T > 2.0$.

Rosenfeld suggested that this disparity occurs as a result of the interpretation of the experimental results (ref. 14). The computed streamline traces represent instantaneous streamlines. The experimental streamline cannot be visualized instantaneously due to the

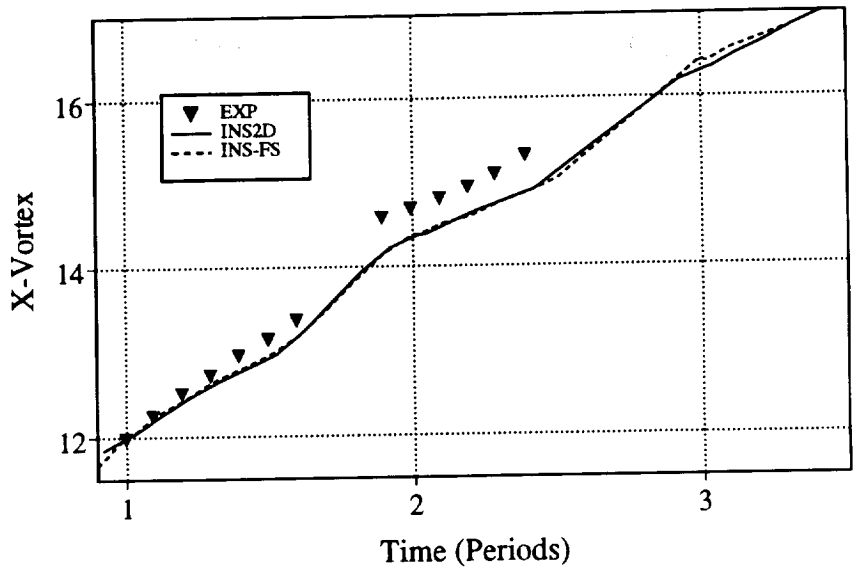

Figure 15. Location of B-vortex versus period: Case I, $Re = 131.9$.

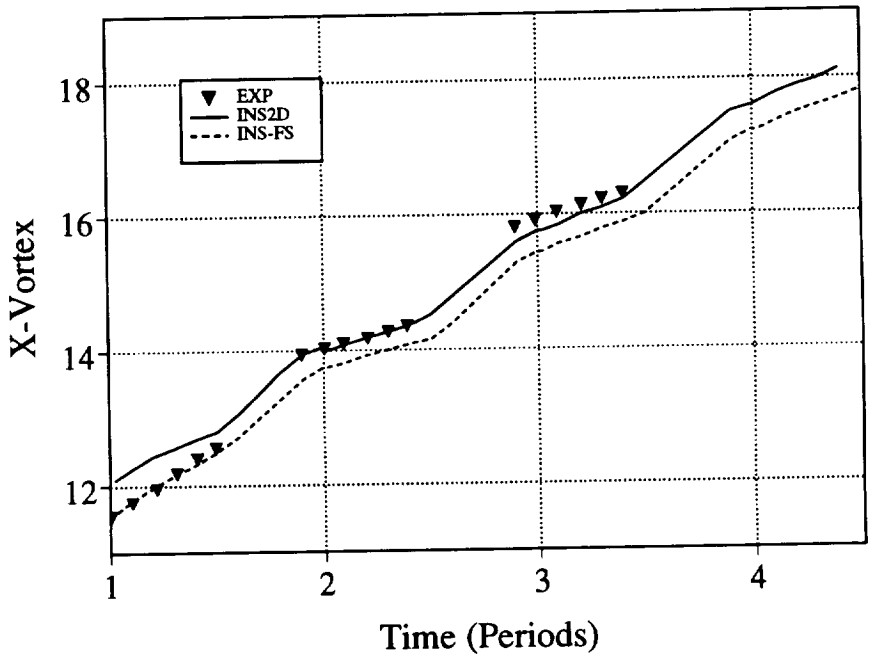

Figure 16. Location of B-vortex versus period: Case II, $Re = 138.3$.

exposure time of the camera taking the streamline data. The estimation of actual physical parameters may affect the comparison of experimental and computed results. The effect of the error tolerances on the experimental results is unknown.

Another area of comparison is the computing time needed to obtain a periodic solution. Rosenfeld (ref. 16) reports the INS3D-FS code requires from $0.3 - 1.0 \times 10^{-3}$ CRAY-XMP CPU sec/mesh-point/time-step, depending on the number of iterations required for the convergence of the Poisson solver. To obtain a periodic solution, the INS2D code required 0.24×10^{-3} CRAY-YMP CPU sec/mesh-point/time-step for Case I, and 0.32×10^{-3} CRAY-YMP CPU sec/mesh-point/time-step for Case II. These cases required about 12 sub-iterations per physical time step. For the purpose of comparison, these cases were computed using the same size physical time steps and the exact same grids that were used in the study by Rosenfeld (ref. 14). Overall, the two different algorithms require the same amount of computing time to obtain a periodic solution.

CONCLUSIONS

A general study to compare and contrast two different algorithms for unsteady, incompressible Navier-Stokes equations was performed. This was accomplished by using the INS2D code to generate computational results for comparison with the computational results of Rosenfeld (ref. 14) and the experimental results of Park (ref. 15). The computational work done by the authors included several parameter studies and the generation of converged, periodic solutions. First, a grid resolution study was performed and an appropriate grid for the constricted channel configuration which sufficiently captured the important flow physics was generated. It was necessary to choose a finely spaced grid with 289×61 grid points in order to compute significant flow structure details which were not adequately resolved by the coarser grids. In addition, the effect of the artificial compressibility coefficient, β, on the speed of convergence and the smoothness of the solution was examined. For this configuration, a large value of β increased the speed of convergence but added "spikes" to the solution; as the value of β was increased, the magnitude of the spikes in the solutions increased. Several ideas were generated to reduce or eliminate the spikes in the solution. Grid refinement was performed by fitting a cubic spline to the streamwise grid lines in the area near the constriction. This grid refinement significantly reduced the magnitude of the spikes in the solution. Next, a study was performed to determine the number of periods the solution must be run out in order to achieve periodicity. After four pulsatile inflow periods, the flow physics in the solution became periodic. The effect of varying the maximum allowable tolerance for the divergence of velocity on solution accuracy was examined. Several cases were run with different values of this parameter, ε_{cont}, and the effect of these different values on accuracy and the amount of CPU time needed to generate a solution was determined. As ε_{cont} was reduced, the solution became more accurate, but also more computationally expensive to compute. In this study, a crossover point occurred at which further reducing the value of ε_{cont} did not increase the accuracy of the solution, but was computationally more expensive. Finally, two converged, periodic solutions were generated and data was saved at each time step in the period for comparison with the computational results of Rosenfeld (ref. 14) and the experimental results of Park (ref. 15).

In comparing the computational results generated by Rosenfeld (ref. 14), using the INS3D-FS code, and the current work, using the INS2D code, it appears that the solutions generated by the INS3D-FS code contain stronger vorticity than those generated by the INS2D code. One area where this is evident is in the skin friction data. The skin friction data shown in figures 12(a)-(d) shows similar locations of the fluctuations in skin friction throughout the period. However, the magnitude of the fluctuations is generally larger in the solutions generated by Rosenfeld (ref. 14) using the INS3D-FS code, which correlates to stronger vorticity in these solutions. Due to a lack of detailed experimental measurements, it is difficult to determine whether the solutions generated by INS3D-FS or INS2D are more correct in terms of flow physics. This dissimilarity is most likely a result of the differencing schemes used by the two methods for the convective terms. The INS3D-FS code uses second-order central differencing on a staggered grid which does not add any artificial dissipation. The convective terms in the INS2D code are differenced using a third-order upwind scheme which does add dissipation. This additional dissipation may account for the difference in vorticity found in the two solutions in the region behind the constriction.

The differencing schemes used for the convective terms comprise only one example of where the two algorithms are distinct, as the overall approaches used in the two methods are vastly different. The common thread in the two algorithms is the starting point of using the incompressible Navier Stokes equations. Starting from these equations, the two methods follow radically different paths. The INS3D-FS code uses an integral formulation of the equations, while the INS2D code uses a differential formulation. Another difference in the two methods is the degree of coupling of these equations. In the current method, the INS2D code, the equations are fully coupled, whereas the equations used in the INS3D-FS code are only partially coupled through the pressure equation. The divergence of velocity criteria is satisfied in two completely different ways by the two methods. The use of a staggered grid approach by the INS3D-FS code, versus a non-staggered grid approach by the INS2D code, included with the use of different implicit schemes and dissimilar differencing schemes, all contribute to the distinctness of the two methods. However, despite all the dissimilarities found in the two methods, the two algorithms generate very similar results, as shown in figures 15 and 16, which illustrate the location of the B-vortex and compare the computed results with experimental data. The two algorithms also generate very similiar streamline plots throughout the period. Overall, the agreement between the computed results of Rosenfeld (ref. 14) and the current work is excellent, and the two algorithms require similar amounts of computing time to obtain a periodic solution.

FUTURE WORK

One area which could be examined is the degree of robustness of the two algorithms. Future work could include checking the robustness of the two codes for larger physical time steps. This could be accomplished by continually increasing the size of the time steps by

a factor of two until the codes suffer a loss in stability. Another area which merits further investigation is grid sensitivity. As the two algorithms employ greatly contrasting spatial differencing schemes, examining the effects of skewness, discontinuities, and singularities in different grid topologies could provide interesting insights into algorithm characteristics. An additional way of examining the robustness of the two codes would be to continually increase the Reynolds number while monitoring the physics as well as the numerical stability of the algorithms.

REFERENCES

1. Chorin, A. J.: A Numerical Method for Solving Incompressible Viscous Flow Problems. Journal of Computational Physics, vol. 2, pp. 12–26, 1967.

2. Chorin, A. J.: Numerical Solutions of the Navier-Stokes Equations. Mathematics of Computation, vol. 22, no. 104, pp. 745-762, 1968.

3. Yanenko, N. N.: The Method of Fractional Steps. Springer-Verlag, Berlin, 1971.

4. Kim, Y. M.; and Gatlin, B.: A Generalized Multi-Block Version of INS3D. AIAA Paper 91-1611-CP, 1991.

5. Rogers, S. E.: On the Use of Implicit Line-Relaxation and Multi-Zonal Computations. AIAA Paper 91-1611-CP, 1991.

6. Ok, H.; and Eberhardt, S.: Solution of Unsteady Incompressible Navier-Stokes Equations Using and LU Decomposition Scheme. AIAA Paper 91-1611-CP, 1991.

7. Park, K. C.; and Matsushima, K.: Stabilization of Divergence-Free Velocity Field Condition for Unsteady Incompressible Flow Computations. AIAA Paper 91-1611-CP, 1991

8. Hafez, M.; and Soliman, M.: Numerical Solution of the Incompressible Navier-Stokes Equations in Primitive Variables on Unstaggered Grids. AIAA Paper 91-1561-CP, June 1991.

9. Williams, M.: The Helmholtz Pressure Method with Algorithms for Nonlinear Fluid-Structure Interaction and Unstructured Meshes. AIAA Paper 91-1565-CP, June 1991.

10. Bell, J. B.; Colella, P.; and Howell, L. H.: An Efficient Second-Order Projection Method for Viscous Incompressible Flow. AIAA Paper 91-1560-CP, June 1991.

11. Shirayama, S.: Local Network Method for Incompressible Navier-Stokes Equations. AIAA Paper 91-1563-CP, June 1991.

12. Chan, D. C.: A Semi-Implicit Indirect Addressing Method for Incompressible Viscous Flow. AIAA Paper 91-1611-CP, June 1991.

13. Mirakhraee, A.; and Davis, S.: Time Accurate Finite Difference Solutions to the Incompressible Navier-Stokes/Energy Equations. AIAA Paper 91-1611-CP, June 1991.

14. Rosenfeld, M.; Stephanoff, K. D.; Park, D. K.; and Kwak, D.: A Numerical and Experimental Simulation of Pulsatile Flow in a Constricted Channel. Proc. 4th International Symposium on Computational Fluid Dynamics, University of California, Davis, Sept. 9–12, 1991.

15. Park, D. K.: The Biofluidmechanics of Arterial Stenoses. M. Sc. Thesis, LeHigh University, Bethlehem, Pennsylvania, 1989.

16. Rosenfeld, M.; Kwak, D.; and Vinokur, M.: A Fractional Step Solution for the Unsteady Incompressible Navier-Stokes Equations in Generalized Coordinate Systems. J. Computational Physics, vol. 94, no. 1, pp. 102–137, Jan. 1991.

17. Rogers, S. E.: Numerical Solutions of the Incompressible Navier-Stokes Equations. NASA TM-102199, 1990.

18. Rogers, S. E.; Kwak, D.; and Kiris, C: Steady and Unsteady Solutions of the Incompressible Navier-Stokes Equations. AIAA J., vol. 29, no. 4, pp. 603–610, April 1991.

REPORT DOCUMENTATION PAGE

Form Approved
OMB No. 0704-0188

1. AGENCY USE ONLY *(Leave blank)*	2. REPORT DATE	3. REPORT TYPE AND DATES COVERED
	November 1993	Technical Memorandum

4. TITLE AND SUBTITLE

A Comparison of Two Incompressible Navier-Stokes Algorithms for Unsteady Internal Flow

5. FUNDING NUMBERS

505-10-01

6. AUTHOR(S)

N. Lyn Wiltberger, Stuart E. Rogers, and Dochan Kwak

7. PERFORMING ORGANIZATION NAME(S) AND ADDRESS(ES)

Ames Research Center
Moffett Field, CA 94035-1000

8. PERFORMING ORGANIZATION REPORT NUMBER

A-94007

9. SPONSORING/MONITORING AGENCY NAME(S) AND ADDRESS(ES)

National Aeronautics and Space Administration
Washington, DC 20546-0001

10. SPONSORING/MONITORING AGENCY REPORT NUMBER

NASA TM-108794

11. SUPPLEMENTARY NOTES

Point of Contact: Stuart E. Rogers, Ames Research Center, MS 239-11, Moffett Field, CA 94035-1000
(415) 604-4481

12a. DISTRIBUTION/AVAILABILITY STATEMENT

Unclassified-Unlimited
Subject Category – 34

12b. DISTRIBUTION CODE

13. ABSTRACT *(Maximum 200 words)*

A comparative study of two different incompressible Navier-Stokes algorithms for solving an unsteady, incompressible, internal flow problem is performed. The first algorithm uses an artificial compressibility method coupled with upwind differencing and a line relaxation scheme. The second algorithm uses a fractional step method with a staggered grid, finite volume approach. Unsteady, viscous, incompressible, internal flow through a channel with a constriction is computed using the first algorithm. A grid resolution study and parameter studies on the artificial compressibility coefficient and the maximum allowable residual of the continuity equation are performed. The periodicity of the solution is examined and several periodic data sets are generated using the first algorithm. These computational results are compared with previously published results computed using the second algorithm and experimental data.

14. SUBJECT TERMS

Navier-Stokes, Artificial compressibility, Unsteady internal flow, Anteriosclerosis

15. NUMBER OF PAGES

26

16. PRICE CODE

A03

17. SECURITY CLASSIFICATION OF REPORT	18. SECURITY CLASSIFICATION OF THIS PAGE	19. SECURITY CLASSIFICATION OF ABSTRACT	20. LIMITATION OF ABSTRACT
Unclassified	Unclassified		